Talanta 234 (2021) 122699

Contents lists available at ScienceDirect

Talanta

journal homepage: www.elsevier.com/locate/talanta

On the performance of carbon-based screen-printed electrodes for (in) organic hydroperoxides sensing in rainwater

Rebeca Jiménez-Pérez [a], Jesús Iniesta [b], María Teresa Baeza-Romero [c], Edelmira Valero [a,*]

[a] Universidad de Castilla-La Mancha. Department of Physical Chemistry. Higher Technical School of Industrial Engineering (ETSIIAB) and Botanical Institute, 02071, Albacete, Spain
[b] Universidad de Alicante. Department of Physical Chemistry and Institute of Electrochemistry, 03690, San Vicente del Raspeig, Alicante, Spain
[c] Universidad de Castilla-La Mancha. Department of Physical Chemistry. School of Industrial and Aerospace Engineering, and Institute of Nanoscience, Nanotechnology and Molecular Materials, 45071, Toledo, Spain

ARTICLE INFO

Keywords:
Carbon-based electrodes
Platinum nanoparticles
Amperometric sensor
Hydroperoxides
Rainwater

ABSTRACT

Hydroperoxides play important roles in atmospheric chemical processes since they act as strong oxidants. This paper details with the modification, characterization and performance of different carbon-based screen-printed electrodes to develop a sensor that allows to analyze organic and inorganic hydroperoxides in atmospheric samples. Commercial electrodes made up of graphite, graphene, carbon nanotubes and graphene oxide were electrochemically activated and subsequently modified by layer-by-layer method with a conducting polymer of azure-A and electrodeposited platinum nanoparticles. Characterization of modified electrodes was performed by FE-SEM, XPS, Raman spectroscopy, cyclic voltammetry, and impedance spectroscopy. Even though all modified carbonaceous substrates enabled the development of competitive electrochemical sensors for (in)organic hydroperoxides detection, carbon nanotubes underlying substrate exhibited the best performances in terms of sensitivity, stability, limit of detection and linear range. This amperometric sensor displayed linear responses to hydroperoxides over 0.081–450 μM with detection limits in the range of 24–558 nM and sensitivity values among 0.0628±1.6E-4 and 0.0112±0.71E-4 μA/μM for the different hydroperoxides herein studied. The developed electrochemical sensor was successfully applied to the analysis of (in)organic hydroperoxides in rainwater samples. Measurements in rainwater were performed in a city located in the East of Spain and collected at two different sites (downtown and suburban area) on two different dates (July and November 2020). The presented results demonstrated high sensitivity and selectivity for the detection of hydroperoxides among a plethora of substances naturally present in rainwater.

1. Introduction

Hydrogen peroxide (H_2O_2) and organic peroxides, especially alkyl hydroperoxides and hydroxyalkyl hydroperoxides, are considered the major oxidants for the conversion of SO_2 to sulfuric acid in aerosols, clouds and rainwater at pH < 5.5 [1–4]. Moreover, hydroperoxides and H_2O_2 are very important oxidants in the atmosphere since they are relevant atmospheric sinks and temporary reservoirs for hydrogen oxide radicals (HOx) and peroxy radicals (ROx) [5], as well as they seem to be key species in secondary organic aerosol (SOA) formation and processing [6].

Hydroperoxides are formed in the atmosphere through the photooxidation and ozonolysis of volatile organic compounds (VOCs). Their major sinks in the gas phase are photolysis, reaction with OH radicals, dry deposition, and wash-out processes by clouds and rainwater [5]. It has been extensively studied that the washout and adsorption processes on watery surfaces are the dominant removal pathways for these atmospheric pollutants [7]. Moreover, these compounds are formed as well *in situ* in the aqueous phase of clouds and rainwater by reactions with the participation of radicals and ionic species [5]. Consequently, the chemical composition of rainwater essentially reflects on the total concentration of hydroperoxides present in the atmosphere [8]. In general, peroxides can be present at concentrations sufficient to induce cell and tissue damage because of their high reactivity and oxidation potential [9]. Therefore, it is of great importance to develop rapid, simple, reliable, and sensitive methods for their detection and

* Corresponding author.
E-mail addresses: Rebeca.Jimenez@uclm.es (R. Jiménez-Pérez), jesus.iniesta@ua.es (J. Iniesta), MariaTeresa.Baeza@uclm.es (M.T. Baeza-Romero), Edelmira.Valero@uclm.es (E. Valero).

https://doi.org/10.1016/j.talanta.2021.122699
Received 25 March 2021; Received in revised form 4 June 2021; Accepted 6 July 2021
Available online 7 July 2021

quantification.

Different techniques have been applied to the measurement of organic hydroperoxides (OHPs) and H_2O_2 in atmospheric samples, among which it is important to mention HPLC coupled to fluorescence detection [10], or peroxidase-based post-column derivatization [11], and more recently gas chromatography coupled to high resolution time of flight mass spectrometry [12]. A traditional technique that has been widely used for quantification of the total peroxide content is iodometry [13]. However, this methodology suffers from artefacts due to the presence of other substances like metals, it lacks of sensitivity to certain peroxides [14] and suffers from oxygen interference that force to make the analysis under anaerobic conditions.

The development of electrochemical sensors has been widely researched as a successful and inexpensive method to detect a variety of organic and inorganic analytes. In this regard, electrochemical enzymatic biosensors have been tested for OHPs determination [15,16]. However, the low enzyme stability and specific activity as well as significant inhibition of the immobilized enzyme caused by the reaction products can influence in the response of this type of sensors [17]. For that reason, substantial research effort has been directed in the last years to look for new alternative materials with enhanced electrical and surface properties [18].

Carbon based electrodes are widely used in electroanalytical investigations for the development of sensors to determine a plethora of organic and inorganic analytes because of their low cost, good electron transfer kinetics and biocompatibility [19–21]. Moreover, modification of the carbonaceous surface is necessary to improve the electrocatalysis towards the electrooxidation of organic and inorganic hydroperoxides. Recently, Jimenez-Perez et al. [22], have developed a highly sensitive non-enzymatic sensor for hydrogen peroxide analysis based on poly (azure A)-platinum nanoparticles electrodeposited on previously activated screen printed carbon electrodes. The combined advantages of the unique properties of each component endowed these modified electrodes with excellent sensing properties in comparison to the as prepared platinum nanoparticle based carbon electrodes [23,24]. Even though the electrochemical conditioning of the carbon underlying substrate seems to be crucial for the performance of the whole electrochemical sensor toward the detection of H_2O_2, upon the electrodeposition of the polymeric layer along with the presence of platinum nanoparticles, the effect of nature, structure and surface chemistry of different carbonaceous materials could dictate the electrochemical outcome of the sensor towards the determination of H_2O_2 and OHPs, respectively. That said, graphene and graphene-based electrodes such as fullerenes, carbon nanotubes, graphene oxide and reduced graphene oxide have emerged in recent years as promising excellent materials in the field of electrochemistry as catalytic supports due to their extraordinary chemical, physical and mechanical properties [25,26]. In this regard, electrochemical deposition of (in)organic materials, such as conjugated polymers and noble metal nanoparticles onto graphene-based surfaces can in some extent decrease overpotentials of many analytically important electrochemical reactions improving the sensor response [27–29].

In this work, we have explored the advantages of forming conducting polymer layers via electropolymerization, doped with platinum nanoparticles on different activated carbonaceous surfaces such as carbon, graphene, carbon nanotubes and graphene oxide with the aim to develop an electrochemical sensor for the determination of not only H_2O_2, but also organic hydroperoxides for the first time. The effect of the different carbonaceous surfaces upon the amperometric response of the electrochemical outcome for the sensing of H_2O_2, *tert*-butyl hydroperoxide (*t*-BuOOH), cumene hydroperoxide (CuOOH) and 2-butanone peroxide (2-BuOOH) was evaluated in terms of sensitivity, limit of detection (LoD) and linear range concentration. Accordingly, the best electrochemical sensor has been evaluated for the determination of (in) organic hydroperoxides present in rainwater samples. In addition, a number of water-soluble chemicals from different nature that can be found in either rainwater or in atmospheric aerosols has been tested, with no significant response in the electrochemical outcome at the concentrations levels used, which were much higher than those typically present in rainwater.

2. Experimental

2.1. Materials

Acetone, azure A (80%), benzaldehyde, 2-butanone peroxide (2-BuOOH), *tert*-butyl hydroperoxide (*t*-BuOOH), chloroplatinic acid hexahydrate (≥99.9%), cumene hydroperoxide (CuOOH), glyoxal, H_2O_2 (35%), 5-hydroxymethyl-2-furaldehyde, iron (III) chloride hexahydrate, 4-methylcatechol, 4-nitrophenol and sodium dodecyl sulfate (SDS 95%) were purchased from Sigma-Aldrich (Madrid, Spain). H_2SO_4 (0.5 M SV) and oxalic acid were obtained from Panreac. Glacial acetic acid (HPLC grade) and KCl from Scharlau (Barcelona, Spain). Benzene, copper (II) sulfate pentahydrate, KH_2PO_4, K_2HPO_4, $K_4Fe(CN)_6$ and HCl (32%) were obtained from Merck, KNO_3 from Fluka (ultra) and ammonium sulfate from Probus. Reagents for the spectrophotometric method for the measurement of hydroperoxides such as bovine serum albumin (BSA), catalase (CAT), ethylenediaminetetraacetic acid disodium salt (EDTA), glutathione peroxidase from bovine erythrocytes (GPx), glutathione reduced (GSH), glutathione reductase from baker's yeast (GR) were also acquired from Sigma-Aldrich; β-nicotinamide adenine dinucleotide reduced disodium salt (β-NADH) was obtained from Roche Diagnostics and tris(hydroxymethyl)-aminomethane from Merck. All chemicals were of analytical grade and of the highest purity available.

Rainwater samples were collected in Albacete, a city located in the central eastern region of Spain (38.9942°N 1.8564°W), by placing an open wide polypropylene bottle (1L) at the ground-floor level of our working center (ETSIIAB building, suburban area) and on the sixth-floor terrace of a downtown building in July and November 2020. Once collected, samples were filtered through a 0.45 μm filter (Filter-Lab® from filter ANOIA), cold stored and analyzed within 12 h after collection with no additional pre-treatment.

2.2. Carbon-based modified electrodes

The electrodes herein used were disposable screen-printed carbon-based electrodes (DropSens). Screen-printed carbon electrodes (DRP-110), graphene modified screen-printed carbon electrodes (DRP-110GPH), multi-walled carbon nanotubes modified screen-printed carbon electrodes (DRP-110CNT) and graphene oxide modified screen-printed carbon electrodes (DRP-110GPHOX) were studied for comparative purposes. All these electrodes have a silver pseudo-reference electrode.

The electrodes DRP-110 (SPCEs), DRP-110GPH (SPGEs) and DRP-110CNT (SPCNTEs) were modified in agreement with the protocol recently reported by Jimenez-Perez et al. [22]. This method consists of three sequential stages: 1_Electrochemical activation of the surface of the electrodes using 10 mM H_2O_2. 2_Electrodeposition of a conductive polymer poly(azure-A) which stands for PAA. 3_Electrogeneration of platinum nanoparticles from platinum solution (H_2PtCl_6). The final obtained electrodes stand for: aSPCE/PAA:Pt, aSPGE/PAA:Pt and aSPCNTE/PAA:Pt, respectively.

As reported by Gonzalez-Sanchez et al. [30], the H_2O_2-induced activation of the carbonaceous surface of the working electrode introduces oxygenated functionalization such as hydroxyl, ketone and/or carboxyl groups. The electrodes DRP-110GPHOX (SPGOEs) have a large amount of oxygenated functional groups on its basal plane and edges [31]. Therefore, SPGOEs were only subjected to steps 2 and 3 (electropolymerization and platinum nanoparticles electrodeposition, respectively). This allowed us to compare both graphene surfaces (aSPGE and SPGOE) as regards the electrodeposition of the composite. The abbreviation used for these modified electrodes was SPGOE/PAA:Pt.

2.3. Physico-chemical characterization of the electrodes

2.3.1. Raman spectrometer

The surface of the modified electrodes was investigated by Raman spectroscopy with a JASCO NRS-5100 Laser Raman spectrometer coupled with a confocal microscope (× 50 objective). The excitation line was provided by a standard laser at 532 nm at a very low power level to avoid heating effects.

2.3.2. XPS spectrometer

The X-ray photoelectronic spectroscopy (XPS) analysis was performed on a K-Alpha Thermo Scientific spectrometer using Al-Kα (1486.6 eV) radiation, monochromatized by a twin crystal monochromator to yield a focused X-ray spot with a diameter of 400 μm mean radius. The alpha hemispherical analyzer was used as an electron energy analyzer that operates in the fixed analyzer transmission mode, with survey scan pass energy of 200 eV and 40 eV narrow scans. Processing of the XPS spectra was performed using the Avantage software, with energy values referenced to the C 1s peak of adventitious carbon located at 284.6 eV.

2.3.3. FE-SEM (The field emission scanning electron microscope)

The morphology of the electrodes was analyzed using field emission scanning electron microscopy (FE-SEM, HITACHI S–3000 N microscope), working at 30 kV with a Bruker Xflash 3001 X-ray detector for the microanalysis.

2.4. Hydroperoxides sensing

2.4.1. Amperometric method

Electrochemical measurements were performed on an AUTOLAB PGSTAT 128 N (Eco Chemie B.V) equipped with a frequency response analyzer (FRA) module controlled by the NOVA 2.0 software package. Unless otherwise indicated, all potentials are referred to the Ag-SPCE pseudo-reference electrode. Before using the electrodes for the first time and after each measurement, the modified electrodes were subjected to electrochemical cleaning in 0.5 M sulfuric acid until a stable cyclovoltammogram profile was obtained (about 20 cycles) between −0.71 V and 1.1 V versus the reference electrode Ag-SPCE.

The amperometric technique was used to evaluate and compare the electrochemical sensor outcomes for the determination of the concentration of H_2O_2 and the following organic hydroperoxides: *tert*-butyl hydroperoxide (*t*-BuOOH), cumene hydroperoxide (CuOOH) and 2-butanone peroxide (2-BuOOH). The polarization potential was fixed at 0.4 V *vs.* the Ag-SPCE pseudo-reference electrode. This potential was chosen after recording the linear scan voltammograms of each compound on each electrode in phosphate buffer 0.1 M (pH 7). The oxidation peaks of the organic compounds ranged between 0.25 and 0.5 V. A potential of 0.4 V was chosen as the minimum potential at which all compounds could be measured with adequate sensitivity. Calibrations were performed individually for each hydroperoxide in a concentration range between 100 nM and 450 μM. For that purpose, the different hydroperoxides were spiked into 5 mL of 0.1 M phosphate buffer pH 7 under magnetic stirring. The current intensity was measured after stabilization.

2.4.2. Spectrophotometric method

Spectrophotometric measurements were carried out with a UV/Vis PerkinElmer Lambda 35 spectrophotometer (PerkinElmer Instruments, Waltham, US). The H_2O_2 -equivalent total hydroperoxides concentration (THPs) in the real samples was additionally measured by an enzymatic method similar to that reported by Heath and Tappel [32]. Briefly, a calibration straight line in the range from 3 μM to 50 μM was obtained with the following assay mixture: 100 mM Tris/HCl buffer with 0.5 mM EDTA, pH 7.6, 100 μM β-NADH, 280 μM GSH, 1.5 units of GPx, 0.5 units of GR and different volumes of a stock solution of 100 μM H_2O_2. The reaction was started by the addition of GR after 10 min of preincubation, the final volume being 500 μl. The time course of the reaction was followed by measuring the disappearance of β-NADH until the end of the reaction at 340 nm (ε = 6270 M^{-1} cm^{-1}) at 33 °C. The difference in absorbance between the beginning and the end of the reaction was plotted against the concentration of H_2O_2 to obtain the calibration straight line.

Rainwater samples were analyzed in triplicate for both electrochemical and spectrophotometric techniques. For the determination of OHPs, samples were previously incubated with catalase for 15 min. H_2O_2 concentration was calculated by the difference between THPs and OHPs. Sensitivity (S) was calculated from the slope of the corresponding calibration straight line, the limit of detection (LoD) and limit of quantification were estimated using 3 and 10 times, respectively, the standard deviation of the blank signal/slope (3 x S_b/m and 10 x S_b/m).

3. Results and discussion

3.1. Surface and structural characterization of the electrodes

Different carbon-based screen-printed electrodes were characterized by FE-SEM, Raman spectroscopy and XPS. It has been demonstrated that the electrochemical response, and therefore the sensor performance is greatly affected by the structure and the surface chemistry of the carbon support [33]. Thus, different techniques and procedures aimed at modulating or manipulating surface functional groups and defects have been studied for decades to enhance the electrochemical activities of carbon substrates [34]. Among these, electrochemical activation of carbonaceous surfaces has proven to be one of the most effective methods of obtaining highly oxygenated surfaces [30,35] as well as an increase in the edges sites generated by an etching effect [36,37].

Fig. 1 shows the morphological FE-SEM images of aSPCE/PAA:Pt (Fig. 1A and B), aSPGE/PAA:Pt (Fig. 1C and D), aSPCNTE/PAA:Pt (Fig. 1E and F) and SPGOE/PAA:Pt (Fig. 1G and H). It is evident from the obtained images that different morphologies arise from the different carbonaceous supports. A more generalized view of these microstructures (Figure S1 in the Supplementary Material) indicates a more uniform dispersion of small Pt nanoparticles on aSPCNTE/PAA:Pt. This distribution of the nanoparticles has been related to an increase in the active surface area [23] as well as a reduction in electrochemical noise and improved sensitivity towards hydrogen peroxide [38].

We also employed Raman spectroscopy to evaluate the structural order of the composites deposited on the different carbonaceous surfaces and the major contributions in the polymeric coating. Fig. 2A shows the Raman spectra of aSPCE/PAA:Pt, aSPGE/PAA:Pt, aSPCNTE/PAA:Pt and SPGOE/PAA:Pt, where typical features of carbonaceous materials are observed in the energy interval between 1200 and 1800 cm^{-1}. The spectra generally exhibited the Raman bands attributed to disordered band (D: 1349 cm^{-1} and D': 1625 cm^{-1}) and ordered band (G: 1585 cm^{-1}) graphene like structures [39] related to the vibrations of sp^2 building blocks. Moreover, intrinsic structural defects can be also observed in a distinct peak at 1500 cm^{-1} related to amorphous sp^2-bonded forms of carbon [40]. However, in this spectral region, there are overlapping bands that were attributed to the electrogenerated polymer on the surfaces. The Raman spectra of aSPCE/PAA:Pt and aSPCNTE/PAA:Pt showed the most intense bands of the polymer composite in the energy interval from 400 to 1500 cm^{-1} suggesting an improved growth of the PAA film on these surfaces. This fact is probably due to a higher density of catalytic sites (edge-plane like sites and tube ends) [39] associated to carbon and carbon nanotubes inks, compared presumably to the higher density of basal-planes present in graphene surfaces which have proven to be more inert [41]. However, the less defined polymer bands besides the most intense D and G bands showed in the Raman spectrum of SPGOE/PAA:Pt point out to a poor affinity of the polymeric film for this surface. The assignment of the polymer bands, marked with asterisk (*), is displayed in Table S1 of the

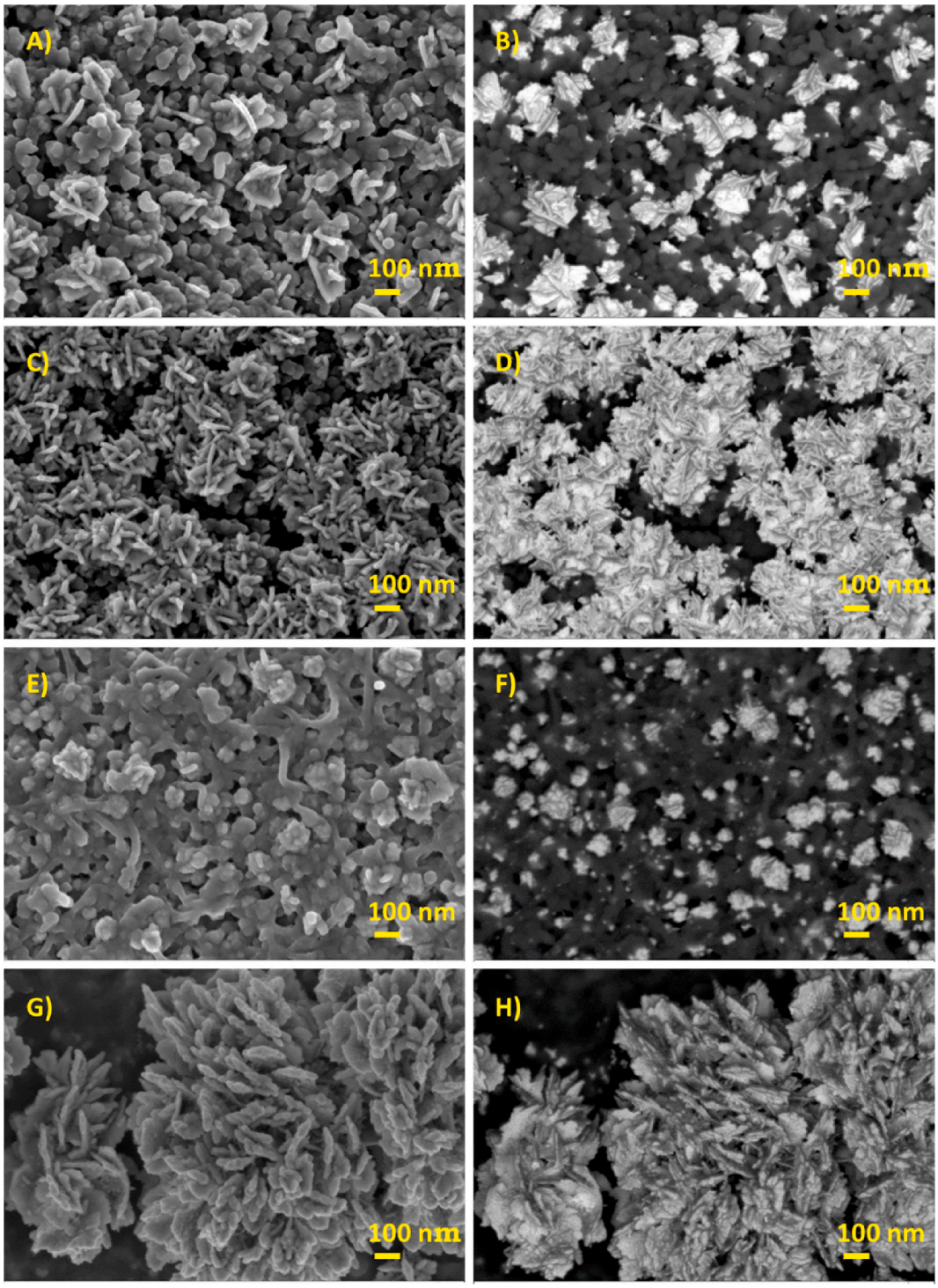

Fig. 1. FE-SEM images of: aSPCE/PAA:Pt (A and B), aSPGE/PAA:Pt (C and D), aSPCNTE/PAA:Pt (E and F) and SPGOE/PAA:Pt (G and H).

Supplementary Material.

The nature of the surface of the polymeric film onto the carbonaceous electrodes was also investigated by XPS. Fig. 2B compiles the data regarding to the relative abundance of C, O, N and S, respectively. Even though the XPS spectra of poly(azure-A) are dominated by a high relative abundance of C for all electrode surfaces, it is worth noting that the contribution of N at.% follows the trend aSPCNTE/PAA:Pt > aSPCE/PAA:Pt > aSPGE/PAA:Pt > SPGOE/PAA:Pt which correlates well with the Raman spectra pattern intensity of the PAA/Pt films shown in Fig. 2A. Moreover, the highest relative abundance of oxygen for the electrode SPGOE/PAA:Pt is probably caused by the contribution of the underlying surface of graphene oxide and therefore the poor electropolymerization yield of poly(azure-A) onto GO; this is confirmed by the presence of a well-defined Raman shift of D and G bands.

XPS spectra were analyzed regarding the relative abundance of nitrogen species after deconvolution of the N 1s core level peak for all the electrodes (Fig. 2C). Data revealed that functional groups linked to pyridinic nitrogen (398.7±0.3 eV) and C–N quaternary (graphitic) (401.3±0.5eV) are dominant in PAA/Pt films performed on carbon and carbon nanotubes based electrodes, namely, for aSPCE/PAA:Pt and

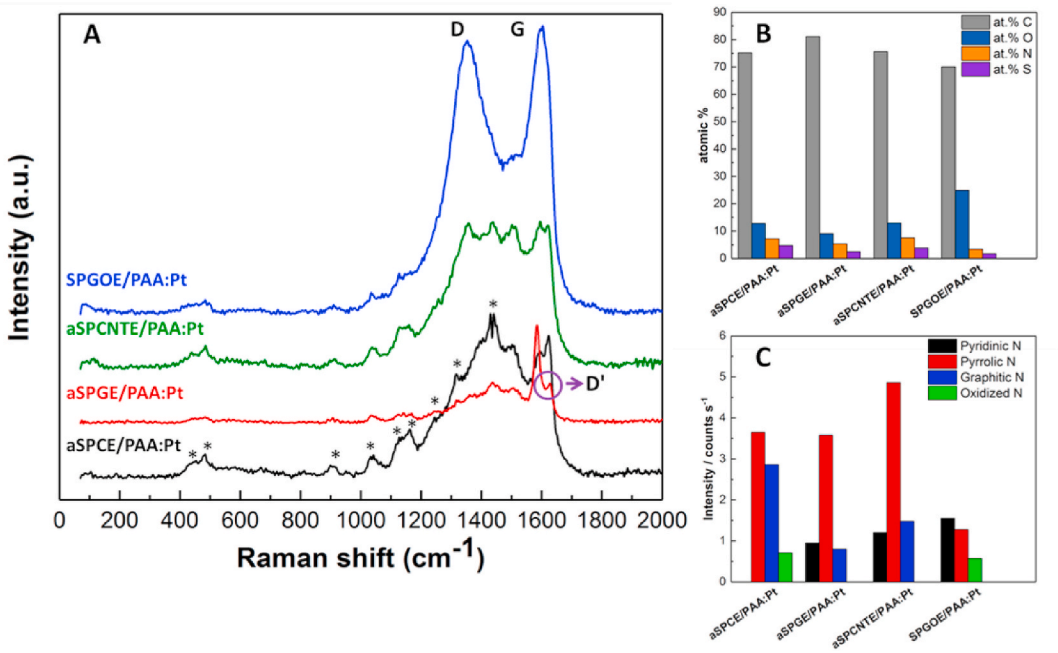

Fig. 2. Raman spectra of the modified electrodes aSPCE/PAA:Pt, aSPGE/PAA:Pt, aSPCNTE/PAA:Pt and SPGOE/PAA:Pt (A). XPS analysis for the modified electrodes aSPCE/PAA:Pt, aSPGE/PAA:Pt, aSPCNTE/PAA:Pt and SPGOE/PAA:Pt in terms of (B) atomic percentage (at.%) of C 1s, O 1s, N 1s and S 2p core levels, (C) relative abundance in at.% of nitrogen groups after deconvolution of N 1s core level.

aSPCNTE/PAA:Pt, whereas that contribution was slightly lower for the aSPGE/PAA:Pt and remarkably reduced for the SPGOE/PAA:Pt. Furthermore, significant changes for all four PAA:Pt films at aSPCE/PAA:Pt, aSPGE/PAA:Pt, aSPCNTE/PAA:Pt and SPGOE/PAA:Pt were centered on the Pt 4f core level peak after deconvolution (Figure S2 in the Supplementary Material). Binding energy peaks at ~71.5 ($4f_{7/2}$) and ~74.5 ($4f_{5/2}$) eV, which are linked to the elemental state Pt^0 [39] (red lines) suggest the preferential formation of platinum in the zero-oxidation state for aSPCE/PAA:Pt, aSPGE/PAA:Pt and SPGOE/-PAA:Pt electrodes. The peaks fitted at ~73.3 ($4f_{7/2}$) and ~77.2 eV ($4f_{5/2}$) (green lines) were assigned to the oxidized states of Pt [42] and could be ascribed to the formation of oxides (PtO_x) and hydroxides ($PtOH_x$) [43,44]. Previous reports [45,46] have proven that the oxidation of hydroperoxides is favoured on oxidized platinum surfaces. The higher Pt^{+2}/Pt^0 ratio of aSPCNTE/PAA:Pt may indicate a preferential formation of oxidized platinum on this electrode. The highest electron density among all surfaces was also found for aSPCNTE/PAA:Pt.

3.2. *Electrochemical characterization and stability of the proposed electrodes*

Electrochemical impedance spectroscopy (EIS) and cyclic voltammetry (CV) experiments were used for the evaluation of the electrochemical interfacial properties of the modified electrodes. Fig. 3 shows the cyclic voltammograms and the EIS behavior of all electrodes tested in this study by using an electrolyte system of 5 mM $[Fe(CN)_6]^{4-}$ (in the presence of 0.1 M KCl) solution. The EIS spectra (Fig. 3A) were taken in a frequency range of 0.01 Hz–65 kHz, applying a constant DC potential of 0.15 V. The diameter of the semicircle in the Nyquist plots provides the value of charge transfer resistance (R_{CT}) which has a direct relationship with the effective charge transfer process of the redox probe at the electrode interface. R_{CT} values of each electrode were found by fitting a Randles type circuit (inset Fig. 3A) to Nyquist curves. The charge transfer resistances of the electrodes are tabulated in Table 1 among their fitting errors. As can be seen the composites aSPGE/PAA:Pt and aSPCNTE/PAA:Pt exhibited the lowest R_{CT} values, indicating better

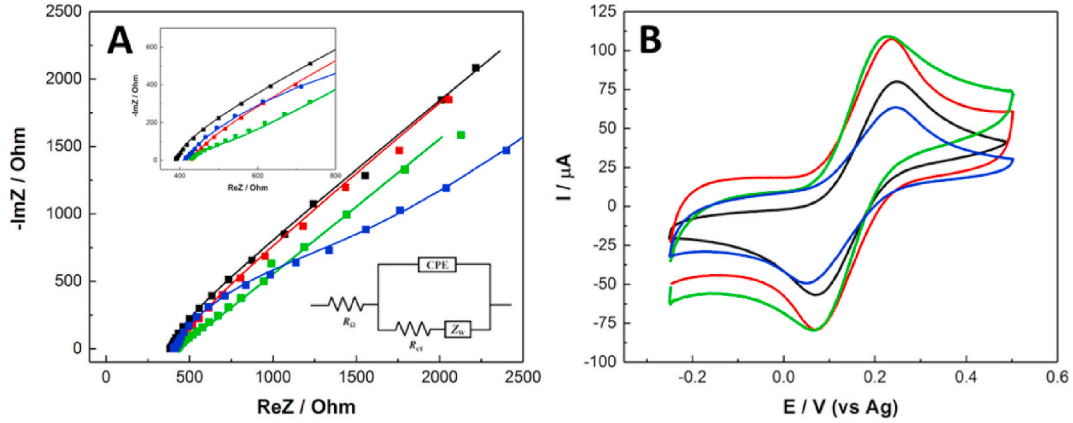

Fig. 3. A) Nyquist plots (Inset: enlarged image at high frequencies) and B) Cyclic voltammograms of the electrodes aSPCE/PAA:Pt (black), aSPGE/PAA:Pt (red), aSPCNTE/PAA:Pt (green) and SPGOE/PAA:Pt (blue) in 5 mM $K_4Fe(CN)_6$ (0.1 M KCl) solution. (For interpretation of the references to colour in this figure legend, the reader is referred to the Web version of this article.)

Table 1
Electrochemical parameters obtained from Fig. 3 and S3.

	R_{CT} (Ω)	ΔEp (V)	Ip_a (μA)	Ip_c (μA)	ECSA (cm^2)	-ΔECSA (%)
aSPCE/ PAA:Pt	120.1 (6.7%)[a]	0.177	80.18	−56.85	2.165	9.1
aSPGE/ PAA:Pt	89.7 (7.3%)[a]	0.162	107.23	−78.58	2.136	36.2
aSPCNTE/ PAA:Pt	98.8 (6.9%)[a]	0.155	109.02	−79.37	2.066	7.8
SPGOE/ PAA:Pt	1289.2 (4.6%)[a]	0.196	63.30	−49.13	0.855	12.6

[a] Fitting errors for $\mathbf{R_{CT}}$.

conductive properties. Other parameters related to the characterization of the surfaces by EIS, such as Y_0 and n, which define the constant phase element (CPE), were also analyzed. For the spectra shown in Fig. 3A, n ranged between 0.92 and 0.98 for aSPCE/PAA:Pt, aSPGE/PAA:Pt and aSPCNTE/PAA:Pt, while for SPGOE/PAA:Pt this value dropped to 0.77. A similar behavior was observed for the parameter Y_0 whose values ranged from 3.99E-4 for SPGOE/PAA:Pt to 6.92E-4 for aSPCNTE/PAA:Pt. These results support the sequence of data obtained for the R_{CT} values with a better electron transfer for the first three electrodes in Table 1. The cyclic voltammetry measurements (Fig. 3B) are also entirely in agreement with the R_{CT} values obtained by EIS where the shift in the anodic and cathodic peaks potentials (ΔEp) is the lowest for aSPGE/PAA:Pt and aSPCNTE/PAA:Pt (Table 1). The last two electrodes exhibited the highest anodic and cathodic peak intensities (Ip_a and Ip_c). These values confirm faster electron transfer reaction kinetics for them.

The modifications performed on the carbonaceous surfaces enable the reuse of the electrodes after electrochemical cleaning in 0.5 M sulfuric acid. Figure S3 shows the voltammograms obtained for the modified electrodes in 0.5 M sulfuric acid, presenting the typical profile for the polycrystalline platinum surfaces in all cases (black lines), though with the evident ohmic drop caused mostly by the shielding effect of the polymeric film. The obtained CV pattern in sulfuric acid barely changed after application to real samples and only a small decrease in current density of the faradaic processes was observed (red lines) after fifteen uses. A use is defined as a set of electrochemical measurements (cyclic voltammetry, linear scan voltammetry or chronoamperometry) (~40–70 consecutive measurements) involving any hydroperoxide or real sample. An electrochemical cleaning was performed after each use. The electrochemically active surface areas (ECSAs) of the working electrodes (tabulated values in Table 1), were determined using the hydrogen adsorption/desorption voltammetric peaks of platinum electrode with a known charge density of 210 μC/cm^2 in 0.5 M H_2SO_4 [47].

To study the stability of the composite, the loss of the electroactive surface area after fifteen uses (electrochemical use and electrochemical cleaning) has been also calculated (-ΔECSA). A significant loss of active platinum surface was observed in aSPGE/PAA:Pt, probably due to a poorer affinity of the polymer with the surface of aSPGE. On the contrary, aSPCE/PAA:Pt and aSPCNTE/PAA:Pt revealed a higher stability with minimal loss of the ECSA value. These data support the previous results obtained by Raman, where it was highlighted that a higher defect density provides a greater number of anchoring groups for the polymer fixation on the carbonaceous surface [48], which would be key issue for the electroanalytical response of the sensor for hydroperoxides determination.

3.3. Analytical performance of the electrodes

The effect of the different carbonaceous surfaces on the amperometric response of the developed sensors in the presence of H_2O_2, *tert*-butyl hydroperoxide (*t*-BuOOH), cumene hydroperoxide (CuOOH) and 2-butanone peroxide (2-BuOOH) was evaluated and compared for all four electrodes. Successive additions of the hydroperoxides (in the range from 10 nM to 100 μM) in phosphate buffer at 0.4 V were performed under magnetic stirring. The calibration plots are presented in Fig. 4. It was found that different starting carbonaceous materials strongly affect analytical performance of the sensor.

To further evaluate the electroanalytical outcomes of the electrodes towards the different hydroperoxides, different analytical parameters including sensitivity, linear range concentration and detection limit are compiled in tables together with their calibration plots (Fig. 4). The best electroanalytical parameters were obtained for the sensing of H_2O_2 followed by CuOOH, 2-BuOOH and *t*-BuOOH. Furthermore, according to the data obtained from the linear regression analysis, it can be seen that the responses achieved by the aSPCNTE/PAA:Pt electrode have the best electroanalytical outcome, which can make it suitable to be used in the determination of H_2O_2 and OHPs in real samples. A comparison of the electroanalytical parameters of these electrodes for OHPs determination with other electrochemical (bio)sensors in aqueous phase is shown in Table 2. The limits of detection and linear ranges attained with the modification herein proposed for OHPs determination are excellent compared with other values reported in the literature in aqueous phase. As regards sensitivities, they are in the same order of magnitude than those obtained with a Prussian-blue electrode, and much better than those obtained with HRP-based biosensors.

FGR-CoPc/GCE: Functionalized Graphene/Cobalt Phtalocyanine/Glassy Carbon Electrode; Pt/poly-N-methylpyrrole-HRP: Poly-N-methylpyrrole-Horseradish Peroxidase onto a Pt electrode; HRP-CPE: Horseradish Peroxidase Carbon Paste Electrode; Pt/PVF/HRP: Horseradish Peroxidase immobilized in a Poly(VinylFerrocenium) film onto a Pt foil electrode; HRP-homopolymer/Pt: Horseradish Peroxidase immobilized on a ferrocene containing siloxane polymer electrochemically deposited onto a Pt electrode; PB-GC: Prussian Blue-Glassy Carbon electrode.

We next turn out to evaluate whether or not the as-prepared electrochemical sensors are capable of determining the total concentration of hydroperoxides (THPs) when they are found together within the same matrix. Fig. 5 shows the amperometric response obtained by successive additions of 10 μM of H_2O_2, CuOOH, 2-BuOOH and *t*-BuOOH, followed by the addition of 2 μM of H_2O_2, CuOOH, 2-BuOOH and *t*-BuOOH and finally, additions of mixtures of the four hydroperoxides, also made in different concentration ratios (see Figure caption).

Comparing the oxidation current responses of the sensors in Fig. 5 with the data obtained from calibration plots in Fig. 4, the relative standard deviations (RSD) for each single measure have been calculated, whose values range from RSD ≤ 5.1% for SPGOE/PAA:Pt to RSD ≤ 1.9% for aSPCNTE/PAA:Pt. These values confirm that the response obtained for the successive additions of the individual hydroperoxides as well as for the mixtures of hydroperoxides are proportional and that make feasible the determination of THPs as the sum of OHPs and H_2O_2 with the proposed electrodes.

3.4. Rainwater samples. Sensitivity and selectivity in aSPCNTE/PAA:Pt

The results obtained up to now compiled in Figs. 4 and 5 suggest that the aSPCNTE/PAA:Pt is the most suitable electrode for the detection of hydroperoxides in real samples. The performance of the electrochemical sensor aSPCNTE/PAA:Pt was validated for the determination of hydroperoxides in rainwater samples freshly collected at different days (see experimental section). To do this, atmospheric H_2O_2 and organic hydroperoxides were measured in samples collected on 14th of July (Fig. 6A) and 4th of November (Fig. 6B) of 2020. Two samples from two different areas of the city were collected at each date. Samples 1 (July) and 1' (November) were taken in the suburbs of Albacete, while samples 2 (July) and 2' (November) were taken in the downtown. Two additions of 300 μL of each rainwater sample, followed by a reference addition of 5 μM of H_2O_2 were carried out up to 4 mL of 0.1 M phosphate buffer (pH 7) under magnetic stirring. THPs concentration was calculated using the aSPCNTE/PAA:Pt calibration curve for H_2O_2. Consequently, the

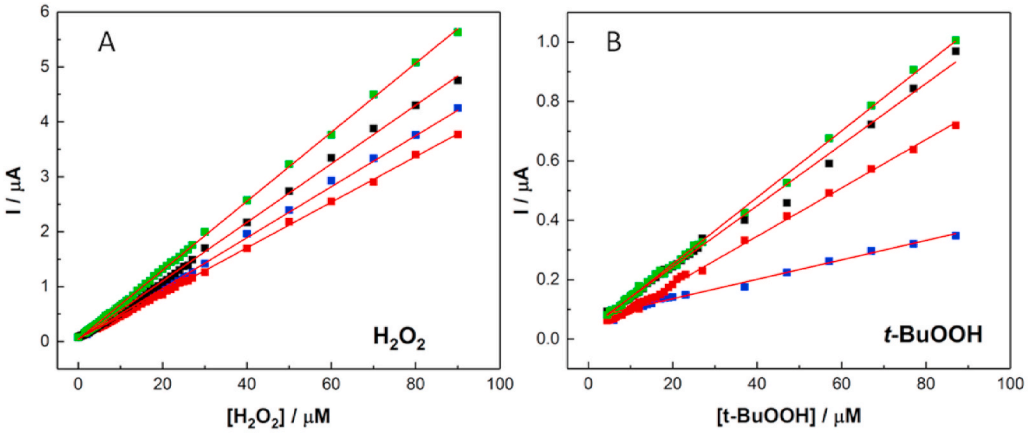

H_2O_2	Linear Range (μM)	LOD (nM)	Sensitivity (μA/μM)
aSPCE/PAA:Pt	0.233-300	69.9	0.0533±2.11E-4
aSPGE/PAA:Pt	0.166-350	50.0	0.0415±1.37E-4
aSPCNTE/PAA:Pt	0.081-450	24.45	0.0628±1.60E-4
SPGOE/PAA:Pt	0.362-330	108.69	0.0470±1.76E-4

t-BuOOH	Linear Range (μM)	LOD (nM)	Sensitivity (μA/μM)
aSPCE/PAA:Pt	1.940-100	1092.1	0.0103±1.26E-4
aSPGE/PAA:Pt	1.861-110	624.7	0.0081±0.57E-4
aSPCNTE/PAA:Pt	1.634-110	558.5	0.0112±0.71E-4
SPGOE/PAA:Pt	2.082-90	3364.6	0.0033±0.93E-4

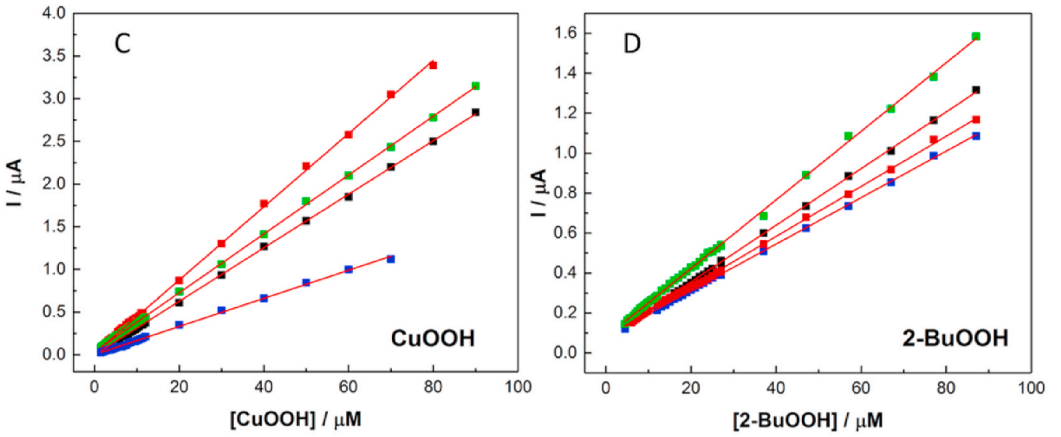

CuOOH	Linear Range (μM)	LOD (nM)	Sensitivity (μA/μM)
aSPCE/PAA:Pt	0.497-100	149.1	0.0314±0.57E-4
aSPGE/PAA:Pt	0.749-80	224.8	0.0429±1.40E-4
aSPCNTE/PAA:Pt	0.492-150	147.6	0.0345±0.63E-4
SPGOE/PAA:Pt	1.243-70	373.0	0.0164±1.02E-4

2-BuOOH	Linear Range (μM)	LOD (nM)	Sensitivity (μA/μM)
aSPCE/PAA:Pt	1.900-150	570.1	0.0142±0.70E-4
aSPGE/PAA:Pt	1.804-150	541.2	0.0125±0.71E-4
aSPCNTE/PAA:Pt	1.246-150	374.0	0.0171±0.73E-4
SPGOE/PAA:Pt	1.541-150	462.3	0.0116±0.49E-4

Fig. 4. Calibration straight lines obtained at 0.4 V *vs* Ag-SPCE for A) H_2O_2, B) *t*-BuOOH, C) CuOOH and D) 2-BuOOH, with the different modified electrodes: aSPCE/PAA:Pt (black), aSPGE/PAA:Pt (red), aSPCNTE/PAA:Pt (green) and SPGOE/PAA:Pt (blue). The tables at the bottom of each figure show the analytical parameters obtained from each calibration straight line. (For interpretation of the references to colour in this figure legend, the reader is referred to the Web version of this article.)

concentrations reported are expressed as H_2O_2-equivalent. With the aim of determining the concentration of OHPs, the same experiment was conducted by previous incubation of the samples with catalase for 10 min. Catalases are distinguished from many other peroxide-metabolizing enzymes by their high specificity for H_2O_2, but weak activity against organic peroxides [53]. Therefore, addition of catalase is a common approach used to remove hydrogen peroxide from samples containing both H_2O_2 and organic hydroperoxides in order to measure organic hydroperoxides total concentration [32,54].

The content of THPs, OHPs and H_2O_2 in samples is shown in Table 3, whose values fall in the average of those recorded in the bibliography [8]. Previous reports published by different research groups show that in general the concentration of H_2O_2 is usually higher than the concentration of organic peroxides in the atmosphere and in rainwater samples. The concentration of organic peroxides in rainwater is usually found in a concentration range between 0.1 and 10 μM [55–57].

In all the samples analyzed the concentration of H_2O_2 is larger than the concentration of OHPs, as proven previously by the literature.

Table 2
Comparative performance of the aSPCNTE/PAA:Pt for OHPs determination in aqueous phase with other electrochemical (bio)sensors.

Electrode	OHP	Sensitivity (μA μM^{-1})	LoD (μM)	Linear range (μM)	Applied Potential	Ref.
FGR-CoPc/GCE	*t*-BuOOH	13.64	5	26–481	−0.5 V (vs. SCE)	[49]
Pt/poly-N-methylpyrrole-HRP	2-BuOOH	$1.49 \cdot 10^{-3}$	0.086	5–85	+0.1 V (vs. Ag/AgCl)	[15]
	t-BuOOH	$5.2 \cdot 10^{-7}$	30	2–48 mM		
HRP-CPE	2-BuOOH	$3.5 \cdot 10^{-3}$	3.1	50–200	−0.2 V (vs. Ag/AgCl)	[50]
	CuOOH	$5.0 \cdot 10^{-4}$	3.3	50–250		
	t-BuOOH	$1.1 \cdot 10^{-4}$	10	50–500		
Pt/PVF/HRP	2-BuOOH	$5.0 \cdot 10^{-3}$ μA μM^{-1} cm^{-2}	–	25–400	+0.7 V (vs. SCE)	[16]
	CuOOH	$3.0 \cdot 10^{-3}$ μA μM^{-1} cm^{-2}	–	100–600		
	t-BuOOH	$2.0 \cdot 10^{-3}$ μA μM^{-1} cm^{-2}	–	100–600		
HRP–homopolymer/Pt	CuOOH	$6.2 \cdot 10^{-10}$	25.5	150–600	−0.05 V (vs. SCE)	[51]
	t-BuOOH	$3.0 \cdot 10^{-11}$	159	50–500		
PB-GC	CuOOH	0.0187	0.35	0.01–0.5 mmol/kg	+0.05 V (vs. Ag/AgCl)	[52]
	t-BuOOH	0.0348	0.2			
aSPCNTE/PAA:Pt	2-BuOOH	0.0171	0.55	1.6–110	+0.4 V (vs. Ag)	This work
	CuOOH	0.0345	0.15	0.5–150		
	t-BuOOH	0.0112	0.37	1.2–150		

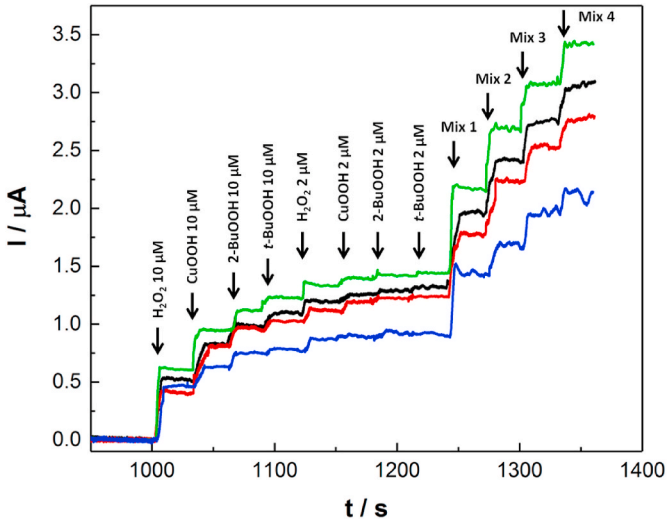

Fig. 5. Amperometric responses of the modified electrodes: aSPCE/PAA:Pt (black), aSPGE/PAA:Pt (red), aSPCNTE/PAA:Pt (green) and SPGOE/PAA:Pt (blue), upon successive additions of both 10 μM and 2 μM of H_2O_2, CuOOH, 2-BuOOH and *t*-BuOOH, and the mixtures in different concentration ratios: Mix 1 (H_2O_2 10 μM + CuOOH 2 μM + 2-BuOOH 2 μM + *t*-BuOOH 2 μM); Mix 2 (H_2O_2 2 μM + CuOOH 10 μM + 2-BuOOH 2 μM + *t*-BuOOH 2 μM); Mix 3 (H_2O_2 2 μM + CuOOH 2 μM + 2-BuOOH 10 μM + *t*-BuOOH 2 μM); Mix 4 (H_2O_2 2 μM + CuOOH 2 μM + 2-BuOOH 2 μM + *t*-BuOOH 10 μM), in phosphate buffer (pH 7) at 0.4 V *vs* Ag-SPCE. (For interpretation of the references to colour in this figure legend, the reader is referred to the Web version of this article.)

Nonetheless, by focusing on the sample collection area of the city, urban area located in the downtown showed higher THPs concentrations (samples 2 and 2′) compared to the suburban area (samples 1 and 1′). These results can be explained by the direct relationship between polluted air, typical of urban areas and highly industrialized regions with high levels of hydroperoxides according to bibliography [7]. As far as the influence of seasonal collection on the THPs is concerned, it is possible to observe a slightly smaller concentration in THPs concentrations in the samples taken in winter (samples 1′ and 2′) compared to summer samples (1 and 2). This observation is in agreement with other studies as local photochemical activity is more pronounced on longer, sunnier days, which substantially increases the concentration of hydroperoxides in the atmosphere [58].

Table 3 also shows a comparison of the results obtained using the electrochemical sensor (aSPCNTE/PAA:Pt) and the spectrophotometric method previously described in the experimental section (2.4.2). The percentage of variation between THPs concentrations measured by both methods ranged from 5.6% to 0.4%. The advantage of taking THPs measurement with aSPCNTE/PAA:Pt benefits from a fast, sensitive and inexpensive methodology when compared with the spectrophotometric method, which suffer longer, expensive measurements as well as being less sensitive at low concentrations, with a narrower linear range. The spectrophotometric determination of OHPs was infeasible, probably due to the organic peroxides concentration was below the quantification limit (BQL) of the method (3.17 μM in the assay reaction mixture).

One of the most important challenges of applying electrochemical sensors to the analysis of real samples refers to the minimization of interfering species within the samples. For that purpose, a number of water-soluble chemicals from different nature that can be found in either rainwater or in atmospheric aerosols was selected. Table S2 shows typical concentrations of these compounds that can be found in rainwater and their importance as part of secondary organic aerosol. Fig. 7 displays the amperometric response of the aSPCNTE/PAA:Pt electrochemical sensor to the consecutive addition of selected chemicals into PBS. In these experiments 5 μM H_2O_2 was added both first and last to ensure the correct functioning of the sensor. Due to the high number of compounds selected for testing as possible interferents, the measurement was carried out in two batches. The first one (black line of Fig. 7) explores the electrochemical outcome of benzene (hydrocarbon), glyoxal, benzaldehyde, 5-hydroxymethyl-2-furaldehyde (aldehydes), acetone (ketone), oxalic acid (carboxylic acid) and 4-methylcatechol (phenolic derivative), all of them with a concentration of 50 μM, which is higher than their typical concentrations in rainwater (see Table S2). The second one (bottom of Figure, red line) explores the electrochemical response of 25 μM 4-nitrophenol, 100 μM acetic acid, 100 μM ammonium sulfate, 10 μM iron(III) chloride, 10 μM copper(II) sulfate, 200 μM potassium chloride and 100 μM potassium nitrate. No increase in the electrochemical signal was detected at the concentrations levels used for these compounds, which were much higher than their typical concentrations in rainwater.

4. Conclusions

Four electrochemical sensors for the detection of hydroperoxides in rainwater have been developed through a series of electrochemical modifications performed onto different carbonaceous surfaces using screen printed electrodes made up of carbon, graphene, carbon nanotubes or graphene oxide as working electrode. The carbonaceous materials were electrochemically activated (except for SPGOE) prior to composite formation through the electrodeposition of a conductive polymer film (PAA) and platinum nanoparticles. The structure, surface chemistry and electrochemical properties of such composites have proven to be linked to the structural characteristics of the underlying carbonaceous substrate. Among all carbon-based composites tested,

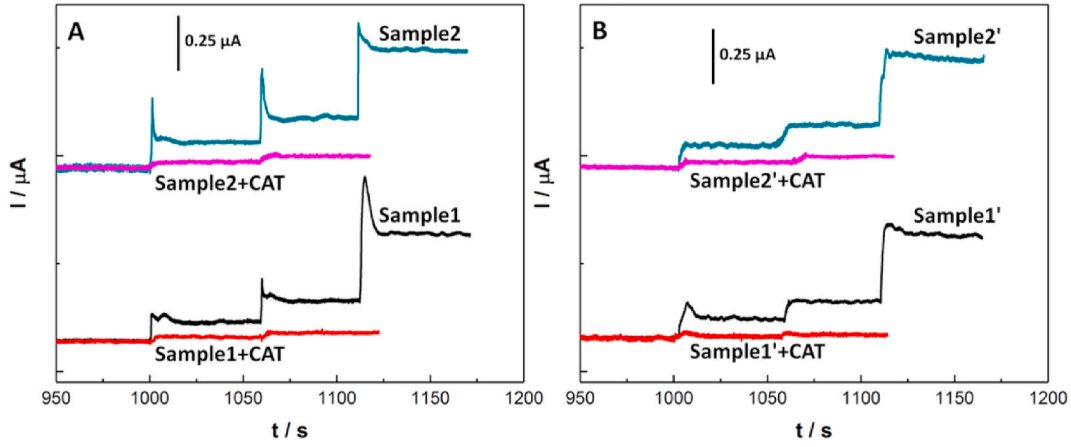

Fig. 6. Amperometric responses of rainwater samples at a aSPCNTE/PAA:Pt collected in A) July and B) November, in Albacete (Spain). Samples 1 and 1' (black lines) were taken in the suburban area of the city and samples 2 and 2' (green line) were taken in downtown. E_{ap} = 0.4 V *vs* Ag-SPCE. (For interpretation of the references to colour in this figure legend, the reader is referred to the Web version of this article.)

Table 3
H_2O_2, OHPs and THPs concentrations found in rainwater samples measured by the electrochemical and spectrophotometric techniques.

	Electrochemistry			Spectrophotometry		
	[THPs] (μM)	[OHPs] (μM)	[H_2O_2] (μM)	[THPs] (μM)	[OHPs] (μM)	[H_2O_2] (μM)
S 1	21.27±0.74	4.44±0.03	16.83±0.77	20.07±1.63	BQL	–
S 2	28.02±1.35	6.56±0.06	21.46±1.41	28.14±0.97	BQL	–
S 1'	18.91±1.65	2.19±0.12	16.73±1.77	19.98±1.13	BQL	–
S 2'	24.32±1.47	5.70±0.19	18.62±1.66	24.42±1.84	BQL	–

BQL: Below the Quantification Limit.

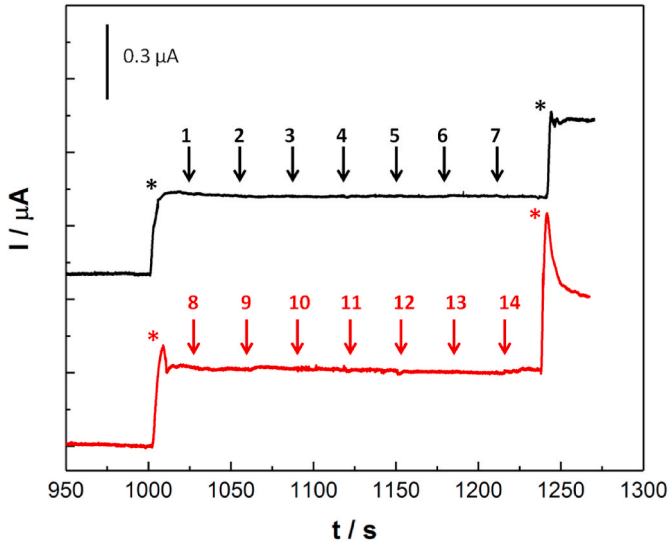

Fig. 7. Amperometric responses of the aSPCNTE/PAA:Pt for the successive addition of 5 μM H_2O_2 (*) and black line: 50 μM of 1) benzene, 2) glyoxal, 3) benzaldehyde, 4) 5-hydroxymethyl-2-furaldehyde, 5) acetone, 6) oxalic acid, 7) 4-methylcatechol and 5 μM H_2O_2 (*). Red line: 8) 25 μM 4-nitrophenol, 9) 100 μM acetic acid, 10) 100 μM ammonium sulfate, 11) 10 μM iron(III) chloride, 12) 10 μM copper(II) sulfate, 13) 200 μM potassium chloride, 14) 100 μM potassium nitrate. E_{ap} = 0.4 V *vs* Ag-SPCE. (For interpretation of the references to colour in this figure legend, the reader is referred to the Web version of this article.)

multi-walled carbon nanotubes based screen printed electrodes (aSPCNTE/PAA:Pt) provided the best electroactivity outcome towards hydroperoxides determination in aqueous solutions in terms of sensitivity, linear concentration range and limit of detection, probably due to a better anchoring of the polymer on this surface according to Raman analysis. Hydroperoxides present in rainwater samples were accurately analyzed by using the electrochemical sensor aSPCNTE/PAA:Pt and data further validated by an spectrophotometric enzymatic method. Electroanalytical data confirmed that the developed electrochemical sensor responds successfully to the (in)organic hydroperoxides determination in rainwater samples, without interfering with other chemical species commonly present in rainwater.

Funding sources

This research was supported by the Spanish Ministry of Science, Innovation and Universities (MICINN, https://www.ciencia.gob.es/) with grants PID2019-106468RB-I00 and PID2019-108136RB-C32, the Junta de Comunidades de Castilla-La Mancha with grant SBPLY/17/180501/000276/2, and the UCLM groups research grants 2020-GRIN-28857 and 2020-GRIN-28771, all of them cofounded with FEDER funds, EU. The funders played no role in study design, in the collection, analysis and interpretation of data, in the writing of the report or in the decision to submit the article for publication.

Credit roles

Rebeca Jiménez-Pérez: Conceptualization, Data curation, Formal analysis, Investigation, Methodology, Validation, Writing – original draft, Writing – review & editing. Jesús Iniesta: Funding acquisition, Project administration, Resources, Supervision, Writing – review & editing. María Teresa Baeza-Romero: Conceptualization, Funding acquisition, Project administration, Supervision, Writing – review & editing. Edelmira Valero: Conceptualization, Funding acquisition, Methodology, Project administration, Resources, Supervision, Validation, Writing – review & editing.

Declaration of competing interest

The authors declare that they have no known competing financial interests or personal relationships that could have appeared to influence the work reported in this paper.

Appendix A. Supplementary data

Supplementary data to this article can be found online at https://doi.org/10.1016/j.talanta.2021.122699.

References

[1] T. Liu, S.L. Clegg, J.P.D. Abbatt, Fast oxidation of sulfur dioxide by hydrogen peroxide in deliquesced aerosol particles, Proc. Natl. Acad. Sci. U.S.A. (2020), https://doi.org/10.1073/pnas.1916401117.

[2] L. Husain, O.V. Rattigan, V. Dutkiewicz, M. Das, C.D. Judd, A.R. Khan, R. Richter, R. Balasubramanian, K. Swami, C.J. Walcek, Case studies of the SO2 + H2O2 reaction in clouds, J. Geophys. Res. Atmos. (2000), https://doi.org/10.1029/1999jd901177.

[3] S.A. Penkett, B.M.R. Jones, K.A. Brice, A.E.J. Eggleton, The importance of atmospheric ozone and hydrogen peroxide in oxidising sulphur dioxide in cloud and rainwater, Atmos. Environ. (2007), https://doi.org/10.1016/j.atmosenv.2007.10.065.

[4] L. Robbin Martin, D.E. Damschen, Aqueous oxidation of sulfur dioxide by hydrogen peroxide at low pH, Atmos. Environ. (1981), https://doi.org/10.1016/0004-6981(81)90146-3.

[5] D.W. Gunz, M.R. Hoffmann, Atmospheric chemistry of peroxides: a review, Atmos. Environ. Part A, Gen. Top. (1990), https://doi.org/10.1016/0960-1686(90)90496-A.

[6] M. Krapf, I. El Haddad, E.A. Bruns, U. Molteni, K.R. Daellenbach, A.S.H. Prévôt, U. Baltensperger, J. Dommen, Labile peroxides in secondary organic aerosol, Inside Chem. (2016), https://doi.org/10.1016/j.chempr.2016.09.007.

[7] R.M. Peña, S. García, C. Herrero, T. Lucas, Measurements and analysis of hydrogen peroxide rainwater levels in a Northwest region of Spain, Atmos. Environ. (2001), https://doi.org/10.1016/S1352-2310(00)00246-6.

[8] X. Lin, L. He, R. Zhang, X. Guo, H. Li, Rainwater in Guangzhou, China: oxidizing properties and physicochemical characteristics, Atmos. Pollut. Res. (2019), https://doi.org/10.1016/j.apr.2018.08.005.

[9] L.A. Morio, K.A. Hooper, J. Brittingham, T.H. Li, R.E. Gordon, B.J. Turpin, D. L. Laskin, Tissue injury following inhalation of fine particulate matter and hydrogen peroxide is associated with altered production of inflammatory mediators and antioxidants by alveolar macrophages, Toxicol. Appl. Pharmacol. (2001), https://doi.org/10.1006/taap.2001.9316.

[10] K. Watanabe, C. Yachi, M. Nishibe, S. Michigami, Y. Saito, N. Eda, N. Yamazaki, T. Hirai, Measurements of atmospheric hydroperoxides over a rural site in central Japan during summers using a helicopter, Atmos. Environ. (2016), https://doi.org/10.1016/j.atmosenv.2016.06.074.

[11] J. Guo, A. Tilgner, C. Yeung, Z. Wang, P.K.K. Louie, C.W.Y. Luk, Z. Xu, C. Yuan, Y. Gao, S. Poon, H. Herrmann, S. Lee, K.S. Lam, T. Wang, Atmospheric peroxides in a polluted subtropical environment: seasonal variation, sources and sinks, and importance of heterogeneous processes, Environ. Sci. Technol. (2014), https://doi.org/10.1021/es403229x.

[12] H. Zhang, L.D. Yee, B.H. Lee, M.P. Curtis, D.R. Worton, G. Isaacman-VanWertz, J. H. Offenberg, M. Lewandowski, T.E. Kleindienst, M.R. Beaver, A.L. Holder, W. A. Lonneman, K.S. Docherty, M. Jaoui, H.O.T. Pye, W. Hu, D.A. Day, P. Campuzano-Jost, J.L. Jimenez, H. Guo, R.J. Weber, J. De Gouw, A.R. Koss, E. S. Edgerton, W. Brune, C. Mohr, F.D. Lopez-Hilfiker, A. Lutz, N.M. Kreisberg, S. R. Spielman, S.V. Hering, K.R. Wilson, J.A. Thornton, A.H. Goldstein, Monoterpenes are the largest source of summertime organic aerosol in the southeastern United States, Proc. Natl. Acad. Sci. U.S.A. (2018), https://doi.org/10.1073/pnas.1717513115.

[13] D.K. Banerjee, C.C. Budke, Spectrophotometric determination of traces of peroxides in organic solvents, Anal. Chem. (1964), https://doi.org/10.1021/ac60210a027.

[14] P. Mertes, L. Pfaffenberger, J. Dommen, M. Kalberer, U. Baltensperger, Development of a sensitive long path absorption photometer to quantify peroxides in aerosol particles (Peroxide-LOPAP), Atmos. Meas. Tech. (2012), https://doi.org/10.5194/amt-5-2339-2012.

[15] E. García-Moreno, M.A. Ruiz, C. Barbas, J.M. Pingarrón, Determination of organic peroxides in reversed micelles with a poly-N-methylpyrrole horseradish peroxidase amperometric biosensor, Anal. Chim. Acta (2001), https://doi.org/10.1016/S0003-2670(01)01311-3.

[16] M. Gündoan-Paul, S.S. Çelebi, H. Özyörük, A. Yldz, Amperometric enzyme electrode for organic peroxides determination prepared from horseradish peroxidase immobilized in poly(vinylferrocenium) film, Biosens. Bioelectron. (2002), https://doi.org/10.1016/S0956-5663(02)00072-6.

[17] E. Shoji, M.S. Freund, Potentiometric sensors based on the inductive effect on the pKa of poly(aniline): a nonenzymatic glucose sensor [3], J. Am. Chem. Soc. (2001), https://doi.org/10.1021/ja005906j.

[18] K. Dhara, D.R. Mahapatra, Recent advances in electrochemical nonenzymatic hydrogen peroxide sensors based on nanomaterials: a review, J. Mater. Sci. (2019), https://doi.org/10.1007/s10853-019-03750-y.

[19] A.C. Power, B. Gorey, S. Chandra, J. Chapman, Carbon nanomaterials and their application to electrochemical sensors: a review, Nanotechnol. Rev. (2018), https://doi.org/10.1515/ntrev-2017-0160.

[20] Y. Liu, D. Wang, L. Xu, H. Hou, T. You, A novel and simple route to prepare a Pt nanoparticle-loaded carbon nanofiber electrode for hydrogen peroxide sensing, Biosens. Bioelectron. (2011), https://doi.org/10.1016/j.bios.2011.05.034.

[21] Y. Sun, K. He, Z. Zhang, A. Zhou, H. Duan, Real-time electrochemical detection of hydrogen peroxide secretion in live cells by Pt nanoparticles decorated graphene-carbon nanotube hybrid paper electrode, Biosens. Bioelectron. (2015), https://doi.org/10.1016/j.bios.2015.01.017.

[22] R. Jiménez-Pérez, J. González-Rodríguez, M.-I. González-Sánchez, B. Gómez-Monedero, E. Valero, Highly sensitive H2O2 sensor based on poly(azure A)-platinum nanoparticles deposited on activated screen printed carbon electrodes, Sensor. Actuator. B Chem. (2019), https://doi.org/10.1016/j.snb.2019.126878.

[23] R. Jiménez-Pérez, L. Almagro, M.I. González-Sánchez, M.Á. Pedreño, E. Valero, Non-enzymatic screen-printed sensor based on PtNPs@polyazure A for the real-time tracking of the H2O2 secreted from living plant cells, Bioelectrochemistry (2020), https://doi.org/10.1016/j.bioelechem.2020.107526.

[24] S.S. Siwal, Q. Zhang, N. Devi, V.K. Thakur, Carbon-based Polymer Nanocomposite for High-Performance Energy Storage Applications, Polymers (Basel), 2020, https://doi.org/10.3390/polym12030505.

[25] D. Chen, L. Tang, J. Li, Graphene-based materials in electrochemistry, Chem. Soc. Rev. (2010), https://doi.org/10.1039/b923596e.

[26] X. Huang, Z. Zeng, Z. Fan, J. Liu, H. Zhang, Graphene-based electrodes, Adv. Mater. (2012), https://doi.org/10.1002/adma.201201587.

[27] C. Tan, X. Huang, H. Zhang, Synthesis and applications of graphene-based noble metal nanostructures, Mater. Today (2013), https://doi.org/10.1016/j.mattod.2013.01.021.

[28] W. Zheng, B. Shen, W. Zhai, Surface functionalization of graphene with polymers for enhanced properties, in: New Prog. Graphene Res., 2013, https://doi.org/10.5772/50490.

[29] G.V. Dubacheva, C.K. Liang, D.M. Bassani, Functional monolayers from carbon nanostructures - fullerenes, carbon nanotubes, and graphene - as novel materials for solar energy conversion, Coord. Chem. Rev. (2012), https://doi.org/10.1016/j.ccr.2012.04.007.

[30] M.I. González-Sánchez, B. Gómez-Monedero, J. Agrisuelas, J. Iniesta, E. Valero, Highly activated screen-printed carbon electrodes by electrochemical treatment with hydrogen peroxide, Electrochem. Commun. (2018), https://doi.org/10.1016/j.elecom.2018.05.002.

[31] J. Chen, Y. Zhang, M. Zhang, B. Yao, Y. Li, L. Huang, C. Li, G. Shi, Water-enhanced oxidation of graphite to graphene oxide with controlled species of oxygenated groups, Chem. Sci. (2016), https://doi.org/10.1039/c5sc03828f.

[32] R.L. Heath, A.L. Tappel, A new sensitive assay for the measurement of hydroperoxides, Anal. Biochem. (1976), https://doi.org/10.1016/0003-2697(76)90277-3.

[33] N. Voeltzel, N. Fillot, P. Vergne, L. Joly, Orders of magnitude changes in the friction of an ionic liquid on carbonaceous surfaces, J. Phys. Chem. C (2018), https://doi.org/10.1021/acs.jpcc.7b10173.

[34] F. Herold, O. Leubner, P. Pfeifer, D. Zakgeym, A. Drochner, W. Qi, B.J.M. Etzold, Synthesis strategies towards amorphous porous carbons with selective oxygen functionalization for the application as reference material, Carbon N. Y (2021), https://doi.org/10.1016/j.carbon.2020.09.030.

[35] M.I. González-Sánchez, M.I. Romero-Llapa, B. Gómez-Monedero, R. Jiménez-Pérez, J. Iniesta, E. Valero, A fast and simple ozone-mediated method towards highly activated screen printed carbon electrodes as versatile electroanalytical tools, Electroanalysis (2019), https://doi.org/10.1002/elan.201900335.

[36] Y. Li, J. Zhou, J. Song, X. Liang, Z. Zhang, D. Men, D. Wang, X.E. Zhang, Chemical nature of electrochemical activation of carbon electrodes, Biosens. Bioelectron. (2019), https://doi.org/10.1016/j.bios.2019.111534.

[37] J.H. Jeong, G.W. Lee, Y.H. Kim, Y.J. Choi, K.C. Roh, K.B. Kim, A holey graphene-based hybrid supercapacitor, Chem. Eng. J. (2019), https://doi.org/10.1016/j.cej.2019.122126.

[38] F. Ai, H. Chen, S.H. Zhang, S.Y. Liu, F. Wei, X.Y. Dong, J.K. Cheng, W.H. Huang, Real-time monitoring of oxidative burst from single plant protoplasts using microelectrochemical sensors modified by platinum nanoparticles, Anal. Chem. (2009), https://doi.org/10.1021/ac901300b.

[39] C.A. Campos-Roldán, G. Ramos-Sánchez, R.G. Gonzalez-Huerta, J.R. Vargas García, P.B. Balbuena, N. Alonso-Vante, Influence of sp3-sp2 carbon nanodomains on metal/support interaction, catalyst durability, and catalytic activity for the oxygen reduction reaction, ACS Appl. Mater. Interfaces (2016), https://doi.org/10.1021/acsami.6b06886.

[40] P. Li, T.J. Zhao, J.H. Zhou, Z.J. Sui, Y.C. Dai, W.K. Yuan, Characterization of carbon nanofiber composites synthesized by shaping process, Carbon N. Y. (2005), https://doi.org/10.1016/j.carbon.2005.05.038.

[41] C.E. Banks, T.J. Davies, G.G. Wildgoose, R.G. Compton, Electrocatalysis at graphite and carbon nanotube modified electrodes: edge-plane sites and tube ends are the reactive sites, Chem. Commun. (2005), https://doi.org/10.1039/b413177k.

[42] K.-C. Pham, D.S. McPhail, C. Mattevi, A.T.S. Wee, D.H.C. Chua, Graphene-carbon nanotube hybrids as robust catalyst supports in proton exchange membrane fuel cells, J. Electrochem. Soc. (2016), https://doi.org/10.1149/2.0891603jes.

[43] M. Kourtelesis, T.S. Moraes, L.V. Mattos, D.K. Niakolas, F.B. Noronha, X. Verykios, The effects of support morphology on the performance of Pt/CeO2 catalysts for the

low temperature steam reforming of ethanol, Appl. Catal. B Environ. (2021), https://doi.org/10.1016/j.apcatb.2020.119757.
[44] X. Liu, Y. Zhou, J. Liu, H. Xia, The intrinsic enzyme mimetic activity of platinum oxide for biosensing of glucose, Spectrochim. Acta Part A Mol. Biomol. Spectrosc. (2021), https://doi.org/10.1016/j.saa.2020.119280.
[45] S.B. Hall, E.A. Khudaish, A.L. Hart, Electrochemical oxidation of hydrogen peroxide at platinum electrodes. Part 1. An adsorption-controlled mechanism, Electrochim. Acta (1997), https://doi.org/10.1016/S0013-4686(97)00125-4.
[46] S.B. Hall, E.A. Khudaish, A.L. Hart, Electrochemical oxidation of hydrogen peroxide at platinum electrodes. Part II: effect of potential, Electrochim. Acta (1998), https://doi.org/10.1016/S0013-4686(97)10116-5.
[47] S. Trasatti, O.A. Petrii, Real surface area measurements in electrochemistry, J. Electroanal. Chem. (1992), https://doi.org/10.1016/0022-0728(92)80162-W.
[48] M.D.L. De La Torre, M.M. Guijarro, Covalent bonds on activated carbon, Eur. J. Org Chem. (2010), https://doi.org/10.1002/ejoc.201000708.
[49] L. Cui, L. Chen, M. Xu, H. Su, S. Ai, Nonenzymatic amperometric organic peroxide sensor based on nano-cobalt phthalocyanine loaded functionalized graphene film, Anal. Chim. Acta (2012), https://doi.org/10.1016/j.aca.2011.11.021.
[50] J. Wang, B. Freiha, N. Naser, E. Gonzalez Romero, U. Wollenberger, M. Ozsoz, O. Evans, Amperometric biosensing of organic peroxides with peroxidase-modified electrodes, Anal. Chim. Acta (1991), https://doi.org/10.1016/0003-2670(91)90012-T.
[51] M.P. García Armada, J. Losada, I. Cuadrado, B. Alonso, B. González, C.M. Casado, J. Zhang, Preparation of biosensors based in a siloxane homopolymer with interacting ferrocenes for the amperometric detection of peroxides, Sensor. Actuator. B Chem. (2004), https://doi.org/10.1016/j.snb.2004.02.043.
[52] N. Adhoum, L. Monser, Electrochemical sensor for hydroperoxides determination based on Prussian blue film modified electrode, Sensor. Actuator. B Chem. (2008), https://doi.org/10.1016/j.snb.2008.03.039.
[53] A. Mhamdi, G. Queval, S. Chaouch, S. Vanderauwera, F. Van Breusegem, G. Noctor, Catalase function in plants: a focus on Arabidopsis mutants as stress-mimic models, J. Exp. Bot. (2010), https://doi.org/10.1093/jxb/erq282.
[54] E.P. Gere, B. Bérczi, P. Simándi, G. Wittmann, A. Dombi, Simultaneous determination of hydrogen peroxide and organic hydroperoxides in water, Int. J. Environ. Anal. Chem. (2002), https://doi.org/10.1080/0306731021000019205.
[55] E. Hellpointner, S. Gäb, Detection of methyl, hydroxymethyl and hydroxyethyl hydroperoxides in air and precipitation, Nature (1989), https://doi.org/10.1038/337631a0.
[56] D. Grossmann, G.K. Moortgat, M. Kibler, S. Schlomski, K. Bächmann, B. Alicke, A. Geyer, U. Platt, M.U. Hammer, B. Vogel, D. Mihelcic, A. Hofzumahaus, F. Holland, A. Volz-Thomas, Hydrogen peroxide, organic peroxides, carbonyl compounds, and organic acids measured at Pabstthum during BERLIOZ, J. Geophys. Res. Atmos. (2003), https://doi.org/10.1029/2001jd001096.
[57] Y.B. Lim, B.J. Turpin, Organic peroxide and OH formation in aerosol and cloud water: laboratory evidence for this aqueous chemistry, Atmos. Chem. Phys. Discuss. (2015), https://doi.org/10.5194/acpd-15-17367-2015.
[58] W. Hua, Z.M. Chen, C.Y. Jie, Y. Kondo, A. Hofzumahaus, N. Takegawa, C.C. Chang, K.D. Lu, Y. Miyazaki, K. Kita, H.L. Wang, Y.H. Zhang, M. Hu, Atmospheric hydrogen peroxide and organic hydroperoxides during PRIDE-PRD'06, China: their concentration, formation mechanism and contribution to secondary aerosols, Atmos. Chem. Phys. (2008), https://doi.org/10.5194/acp-8-6755-2008.